LETTER

doi:10.1038/nature25450

Emergent constraint on equilibrium climate sensitivity from global temperature variability

Peter M. Cox[1], Chris Huntingford[2] & Mark S. Williamson[1]

Equilibrium climate sensitivity (ECS) remains one of the most important unknowns in climate change science. ECS is defined as the global mean warming that would occur if the atmospheric carbon dioxide (CO_2) concentration were instantly doubled and the climate were then brought to equilibrium with that new level of CO_2. Despite its rather idealized definition, ECS has continuing relevance for international climate change agreements, which are often framed in terms of stabilization of global warming relative to the pre-industrial climate. However, the 'likely' range of ECS as stated by the Intergovernmental Panel on Climate Change (IPCC) has remained at 1.5–4.5 degrees Celsius for more than 25 years[1]. The possibility of a value of ECS towards the upper end of this range reduces the feasibility of avoiding 2 degrees Celsius of global warming, as required by the Paris Agreement. Here we present a new emergent constraint on ECS that yields a central estimate of 2.8 degrees Celsius with 66 per cent confidence limits (equivalent to the IPCC 'likely' range) of 2.2–3.4 degrees Celsius. Our approach is to focus on the variability of temperature about long-term historical warming, rather than on the warming trend itself. We use an ensemble of climate models to define an emergent relationship[2] between ECS and a theoretically informed metric of global temperature variability. This metric of variability can also be calculated from observational records of global warming[3], which enables tighter constraints to be placed on ECS, reducing the probability of ECS being less than 1.5 degrees Celsius to less than 3 per cent, and the probability of ECS exceeding 4.5 degrees Celsius to less than 1 per cent.

Many attempts have been made to constrain ECS, typically using either the record of historical warming or reconstructions of past climates[4]. Methods based on historical warming are affected by uncertainties in ocean heat uptake and the contribution of aerosols to net radiative forcing[5,6]. These methods also diagnose the effective climate sensitivity over the historical period, which may be different to ECS, owing to the strength of climate feedbacks varying with the evolving pattern of surface temperature change[4,7–9]. Although methods based on past climatic periods, such as the Last Glacial Maximum[10], are more closely related to the concept of equilibrium, they suffer instead from even larger uncertainties in the reconstruction of net radiative forcing.

As an alternative, the emergent constraint approach uses an ensemble of complex Earth system models to estimate the relationship between a modelled but observable variation in the Earth system and a predicted future change[2,11]. The model-derived emergent relationship can then be combined with the quantification of the observed variation to produce an emergent constraint on the predicted future change[2,11,12]. Here we present an emergent constraint on ECS that is based on the variability of global-mean temperature.

To inform our search for an emergent constraint, we consider the simple 'Hasselmann model'[13] for the variation in global mean temperature ΔT in response to a radiative forcing Q:

$$C\frac{\mathrm{d}\Delta T}{\mathrm{d}t} = Q - \lambda\Delta T = N \quad (1)$$

The constant heat capacity C in this model is a simplification that is known to be a poor representation of ocean heat uptake on longer timescales[14–16]. However, we find that it still offers very useful guidance about global temperature variability on shorter timescales. The climate

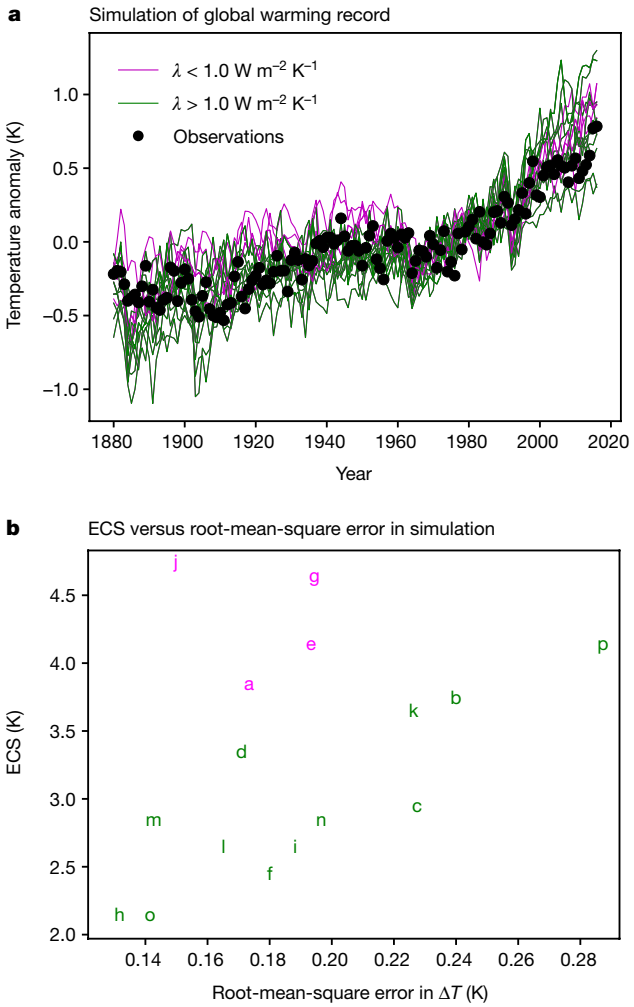

Figure 1 | Historical global warming. a, Simulated change in global temperature from 16 CMIP5 models (coloured lines), compared to the global temperature anomaly from the HadCRUT4 dataset (black dots). The anomalies are relative to a baseline period of 1961–1990. The model lines are colour-coded, with lower-sensitivity models ($\lambda > 1\,\mathrm{W\,m^{-2}\,K^{-1}}$) shown by green lines and higher-sensitivity models ($\lambda < 1\,\mathrm{W\,m^{-2}\,K^{-1}}$) shown by magenta lines. **b**, Scatter plot of each model's ECS against the root-mean-square error in the fit of each model to the observational record. Individual CMIP5 model runs are denoted by the letters listed in Extended Data Table 1.

[1]College of Engineering, Mathematics and Physical Science, University of Exeter, Exeter EX4 4QF, UK. [2]Centre for Ecology and Hydrology, Wallingford OX10 8BB, UK.

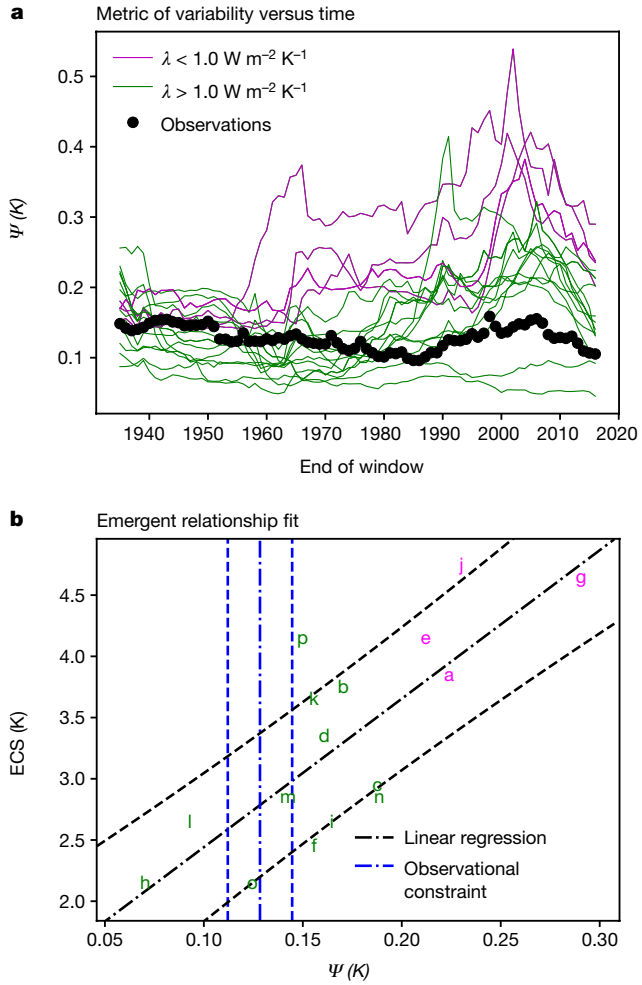

Figure 2 | Metric of global mean temperature variability. a, Ψ metric of variability versus time, from the CMIP5 models (coloured lines), and the HadCRUT4 observational data (black circles). The Ψ values are calculated for windows of width 55 yr, after linear de-trending in each window. These 55-yr windows are shown for different end times. As in Fig. 1, lower-sensitivity models ($\lambda > 1\,\mathrm{W\,m^{-2}\,K^{-1}}$) are shown by green lines and higher-sensitivity models ($\lambda < 1\,\mathrm{W\,m^{-2}\,K^{-1}}$) are shown by magenta lines. **b**, Emergent relationship between ECS and the Ψ metric. The black dot-dashed line shows the best-fit linear regression across the model ensemble, with the prediction error for the fit given by the black dashed lines (see Methods). The vertical blue lines show the observational constraint from the HadCRUT4 observations: the mean (dot-dashed line) and the mean plus and minus one standard deviation (dashed lines).

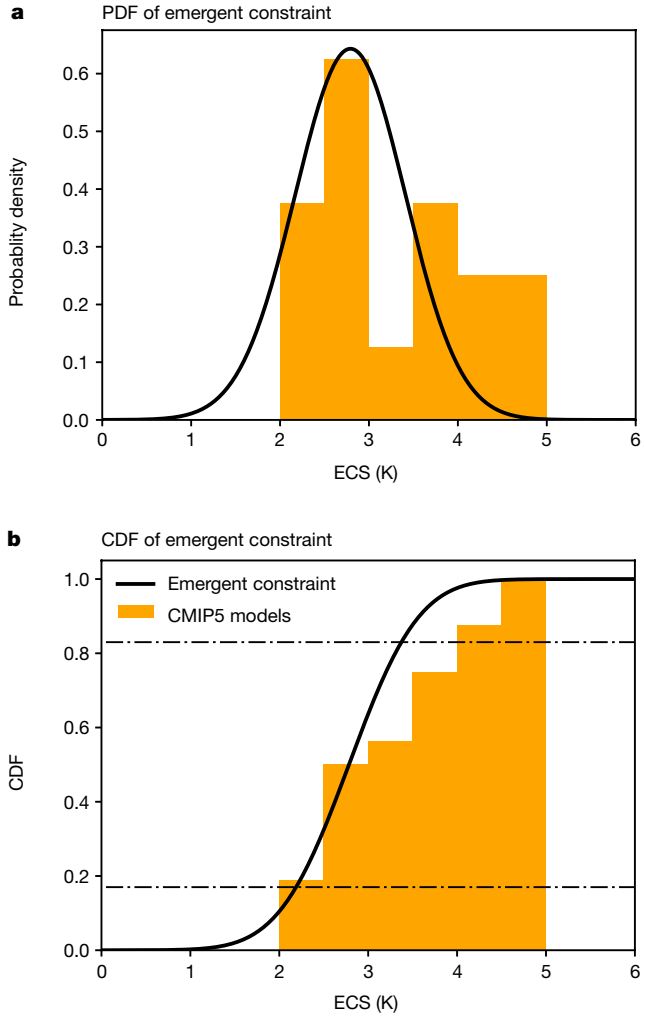

Figure 3 | Emergent constraint on ECS. a, The PDF for ECS. **b**, The related CDF. The horizontal dot-dashed lines show the 66% confidence limits on the CDF plot. The orange histograms (both panels) show the prior distributions that arise from equal weighting of the CMIP5 models in 0.5 K bins.

feedback factor λ determines how the net top-of-atmosphere planetary energy balance N varies with temperature change ΔT in response to a radiative forcing change Q. ECS and λ are inversely related, with a constant of proportionality that is the radiative forcing due to doubling of atmospheric CO_2, $Q_{2\times CO2}$ so that $\mathrm{ECS} = Q_{2\times CO2}/\lambda$. Although the diagnosed $Q_{2\times CO2}$ varies across the model ensemble[17], the uncertainty in ECS is predominantly due to uncertainty in λ, which varies from $0.6\,\mathrm{W\,m^{-2}\,K^{-1}}$ to $1.8\,\mathrm{W\,m^{-2}\,K^{-1}}$, as shown in Extended Data Table 1.

If Q can be approximated as white-noise forcing with variance σ_Q^2, the Hasselmann model can be solved to give expressions for the variance of global temperature σ_T^2 and the one-year-lag autocorrelation of the global temperature α_{1T}, which can be combined to yield an equation for ECS (see Methods):

$$\mathrm{ECS} = \sqrt{2}\,Q_{2\times CO2}\left\{\frac{\sigma_T}{\sigma_Q}\right\}\frac{1}{\sqrt{-\log_e \alpha_{1T}}} = \sqrt{2}\,\frac{Q_{2\times CO2}}{\sigma_Q}\Psi \qquad (2)$$

where $\Psi = \sigma_T/\sqrt{-\log_e \alpha_{1T}}$ is our key metric of global temperature variability. This equation is essentially a fluctuation–dissipation relationship[18] relating the variability of the climate (σ_Q, σ_T, α_{1T}) to its sensitivity to external forcing (ECS).

Observational records of global mean temperature change[3] enable Ψ to be estimated for the real world. The variance of the net radiative forcing is approximately equal to the variance of the top-of-the-atmosphere flux σ_N^2, which can in principle be estimated from satellite measurements. However, the available satellite records are currently too short to provide reliable estimates of σ_N. In addition, the radiative forcing due to doubling CO_2 ($Q_{2\times CO2}$) is not observable in the real world. This means that the right-hand side of equation (2) cannot be directly estimated from observations. Fortunately, we find that the variation in ECS is weakly correlated with $Q_{2\times CO2}/\sigma_N$ across the model ensemble (see Extended Data Table 1). We can therefore approximate the predicted gradient of the ECS versus Ψ emergent relationship using the ensemble mean value of $Q_{2\times CO2}/\sigma_N$ (= 8.7). Our theory therefore predicts a gradient of the ECS versus Ψ emergent relationship of $8.7\sqrt{2} = 12.2$.

Figure 1a shows the simulation of global warming in the historical simulations with the 16 models in the CMIP5 ensemble[19,20] used here (see list in Extended Data Table 1). Here and throughout, higher-sensitivity models ($\lambda < 1.0\,\mathrm{W\,m^{-2}\,K^{-1}}$) are shown in magenta and

lower-sensitivity models ($\lambda > 1.0\,W\,m^{-2}\,K^{-1}$) are shown in green. Observations from the HadCRUT4 dataset[3] are shown by the black line marked with dots. Figure 1a illustrates that both high- and low-sensitivity models are able to fit the historical record with reasonable fidelity, despite implying very different future climates. Models with higher ECS values also have longer response times, and there are variations across the models in net radiative forcing and in ocean heat uptake—allowing models with both high and low sensitivities to reproduce historical global warming[21]. As a result, the fit to the global temperature record does not provide a direct constraint on ECS, as shown in Fig. 1b.

To test whether variability is a better constraint on ECS, we de-trend the global mean temperature records from the models and the observations. Our approach to de-trending is informed by techniques designed to detect precursors of potential tipping points[22] such as 'critical slowing down'[23]. The method applied in that case is to use a moving window, to linearly de-trend within that window, and then to calculate statistics of the de-trended residuals. For tipping point detection, the favoured variable is often the autocorrelation, which measures the memory in fluctuations of the analysed variable[23]. We use a similar approach, although here we apply it to analyse the relationship between Ψ and ECS across the ensemble of models, rather than to detect declining system resilience in a single realization of the system.

We analyse the annual-mean global-mean temperature time series from 16 CMIP5 historical simulations and compare to the HadCRUT4 observational dataset. Although there were another 23 historical runs available in the CMIP5 archive, we chose to use just one model variant from each climate centre, to avoid biasing the emergent constraint towards the centres with the most model runs in the archive. Where there was more than one model variant from a modelling centre, we took the model variant from that centre that had the smallest root-mean-square (r.m.s.) error in the fit to the record of observed global warming from 1880 to 2016. The remaining 23 model runs (which included some initial condition ensembles) were subsequently used to test the robustness of the emergent constraint (see Extended Data Fig. 1).

Figure 2a shows the resulting variation in Ψ for each of the models and the observations, using a window width of 55 yr, and data from 1880 to 2016 to match the available observational datasets. Although Ψ varies in time, the different models are clearly distinguished, in contrast to the simulations of historical global warming (Fig. 1a). In particular, the Ψ values separate higher-sensitivity models (magenta lines) from lower-sensitivity models (green lines), with higher-sensitivity models producing larger Ψ values. It is also worth noting that Ψ from the observational data are within the range of the lower-sensitivity models but clearly outside the range of the higher-sensitivity models. Figure 2b shows the emergent relationship between ECS and the time-mean Ψ values across the model ensemble, with a best-fit gradient that is very close to our theoretical value. The vertical blue lines show the observational constraint on Ψ from the HadCRUT4 dataset, but similar observational constraints are also derived from other datasets of global mean temperature (see Extended Data Table 2).

As in previous studies[11,12] the emergent relationship from the historical runs and observational constraint can be combined to provide an emergent constraint on ECS. This involves convolving the prediction error implied by the fit of the scatter plot to the emergent relationship, with the uncertainty in the observations, to produce a probability density function (PDF) for the y-axis variable (see Methods). Figure 3a shows the resulting PDF for ECS (black curve). For comparison, the prior PDF implied by the equal-weighted model ensemble is shown by the orange histogram. The emergent constraint PDF is sharply peaked around a best estimate of ECS = 2.8 K, which is slightly smaller than the centre of the IPCC range of 1.5–4.5 K. Our best estimate of ECS is considerably larger than the values derived from raw energy budget constraints[8,24,25] but similar to some recent

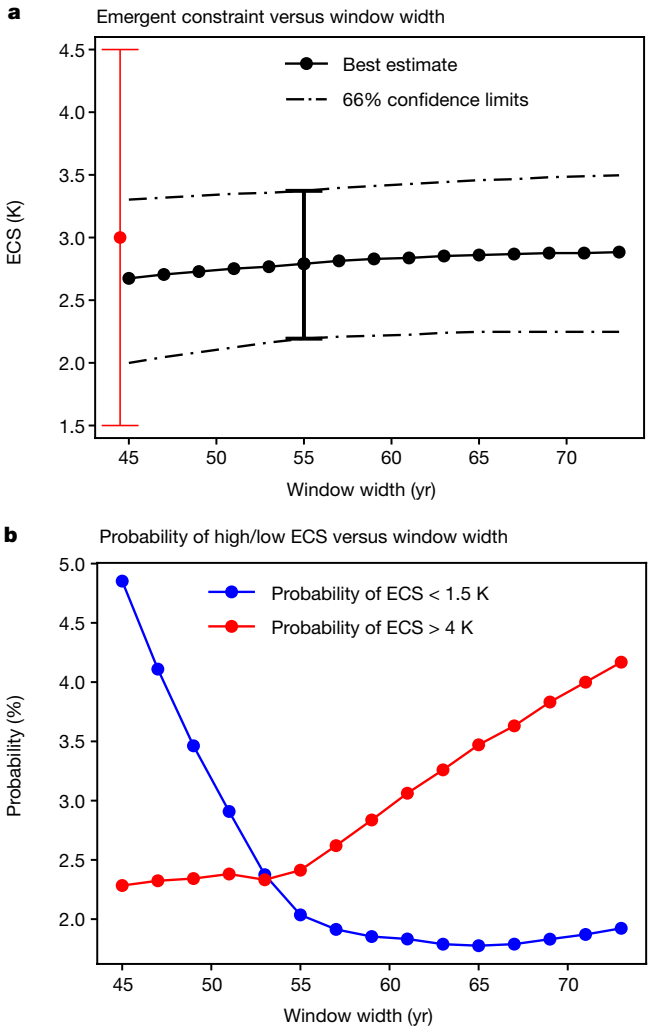

Figure 4 | Sensitivity of the emergent constraint on ECS to window width. a, Central estimate and 66% confidence limits. The thick black bar shows the minimum uncertainty at a window width of 55 yr and the red bar shows the equivalent 'likely' IPCC range of 1.5–4.5 K. **b**, Probabilities of ECS > 4 K (red line and symbols) and ECS < 1.5 K (blue line and symbols).

estimates that account for time-dependent and forcing-dependent feedbacks[9,26].

Figure 3b shows the resulting cumulative density function (CDF), which gives the probability of ECS taking a value lower than the value shown on the x axis. The black horizontal lines in Fig. 3b show the 66% confidence limits (2.2 K to 3.4 K), or approximately 2.8 ± 0.6 K. Relative to the IPCC range of 1.5–4.5 K, this constraint on ECS therefore reduces the uncertainty by about 60%. Indeed, even the 95% confidence limits from the emergent constraint (1.6 K to 4.0 K) fit well within the IPCC 'likely' range for ECS. Our constraint is therefore at odds with a suggestion that the lower 66% confidence limit for ECS could be as high as 3 K (ref. 27). If we instead use all 39 historical runs in the CMIP5 archive, we find a slightly weaker emergent relationship, but derive a very similar emergent constraint on ECS (Extended Data Table 2). The constraint is also robust to the choice of observational dataset, and to whether or not the model global temperature is calculated just across the points where there were observations[28] (Extended Data Table 2 and Extended Data Fig. 2).

Our choice of window width was informed by sensitivity studies in which the emergent constraint was calculated for a range of this parameter. Figure 4a shows the best estimate and 66% confidence limits on ECS as a function of the width of the de-trending window. Our best estimate is

relatively insensitive to the chosen window width, but the 66% confidence limits show a greater sensitivity, with the minimum in uncertainty at a window width of about 55 yr (as used in the analysis above). As Extended Data Fig. 3 shows, at this optimum window width the best-fit gradient of the emergent relationship between ECS and Ψ (= 12.1) is also very close to our theory-predicted value of $\sqrt{2}\,Q_{2\times CO2}/\sigma_Q$ (= 12.2). This might be expected if this window length optimally separates forced trend from variability.

Figure 4b shows the probability of ECS > 4 K and ECS < 1.5 K as a function of window width. For comparison, the IPCC 'likely' range of 1.5–4.5 K implies a 25% probability of ECS > 4 K, and a 16% probability of ECS < 1.5 K. At the optimum window width of 55 yr, both probabilities are close to their minimum values of less than 2.5%. Our emergent constraint therefore greatly reduces the uncertainty in the ECS value of Earth's climate, implying a less than 1 in 40 chance of ECS > 4 K, and renewing hope that we may yet be able to avoid global warming exceeding 2 K.

Online Content Methods, along with any additional Extended Data display items and Source Data, are available in the online version of the paper; references unique to these sections appear only in the online paper.

Received 27 July; accepted 13 December 2017.

1. Collins, M. *et al.* Long-term climate change: projections, commitments and irreversibility. In *Climate Change 2013: The Physical Science Basis. Contribution of Working Group I to the Fifth Assessment Report of the Intergovernmental Panel on Climate Change* (eds Stocker, T. F. *et al.*) Ch. 12 (Cambridge Univ. Press, 2013).
2. Hall, A. & Qu, X. Using the current seasonal cycle to constrain snow albedo feedback in future climate change. *Geophys. Res. Lett.* **33,** L03502 (2006).
3. Morice, C. P. *et al.* Quantifying uncertainties in global and regional temperature change using an ensemble of observational estimates: the HadCRUT4 dataset. *J. Geophys. Res.* **117,** D08101 (2012).
4. Knutti, R. *et al.* Beyond equilibrium climate sensitivity. *Nat. Geosci.* **10,** 727–736 (2017).
5. Gregory, J. M. *et al.* An observationally based estimate of the climate sensitivity. *J. Clim.* **15,** 3117–3121 (2002).
6. Forster, P. M. *et al.* Evaluating adjusted forcing and model spread for historical and future scenarios in the CMIP5 generation of climate models. *J. Geophys. Res. Atmos.* **118,** (2013).
7. Gregory, J. M. & Andrews, T. Variation in climate sensitivity and feedback parameters during the historical period. *Geophys. Res. Lett.* **43,** 3911–3920 (2016).
8. Forster, P. M. Inference of climate sensitivity from analysis of Earth's radiation budget. *Ann. Rev. Earth Planet. Sci.* **44,** 85–106 (2016).
9. Armour, K. C. Energy budget constraints on climate sensitivity in light of inconstant climate feedbacks. *Nat. Clim. Chang.* **7,** 331–335 (2017).
10. Annan, J. D. & Hargreaves, J. C. Using multiple observationally-based constraints to estimate climate sensitivity. *Geophys. Res. Lett.* **33,** L06704 (2006).
11. Cox, P. M. *et al.* Sensitivity of tropical carbon to climate change constrained by carbon dioxide variability. *Nature* **494,** 341–344 (2013).
12. Wenzel, S. *et al.* Projected land photosynthesis constrained by changes in the seasonal cycle of atmospheric CO_2. *Nature* **538,** 499–501 (2016).
13. Hasselmann, K. Stochastic climate models. I. Theory. *Tellus* **28,** 473–485 (1976).
14. MacMynowski, D. G. *et al.* The frequency response of temperature and precipitation in a climate model. *Geophys. Res. Lett.* **38,** L16711 (2011).
15. Caldeira, K. & Myhrvold, N. P. Projections of the pace of warming following an abrupt increase in atmospheric carbon dioxide concentration. *Environ. Res. Lett.* **8,** 034039 (2013).
16. Geoffroy, O. *et al.* Transient climate response in a two-layer energy-balance model. Part I: Analytical solution and parameter calibration using CMIP5 AOGCM experiments. *J. Clim.* **26,** 1841–1857 (2013).
17. Flato, G. *et al.* Evaluation of climate models. In *Climate Change 2013: The Physical Science Basis. Contribution of Working Group I to the Fifth Assessment Report of the Intergovernmental Panel on Climate Change* (eds Stocker, T. F. *et al.*) Ch. 9 (Cambridge Univ. Press, 2013).
18. Leith, C. E. Climate response and fluctuation dissipation. *J. Atmos. Sci.* **32,** 2022–2026 (1975).
19. Taylor, K. E., Stouffer, R. J. & Meehl, G. A. An overview of CMIP5 and the experiment design. *Bull. Am. Meteorol. Soc.* **93,** 485–498 (2012).
20. Andrews, T. *et al.* Forcing, feedbacks and climate sensitivity in CMIP5 coupled atmosphere-ocean models. *Geophys. Res. Lett.* **39,** L09712 (2012).
21. Kiehl, J. T. Twentieth century climate model response and climate sensitivity. *Geophys. Res. Lett.* **34,** L22710 (2007).
22. Lenton, T. M. *et al.* Tipping elements in the Earth's climate system. *Proc. Natl Acad. Sci. USA* **105,** 1786–1793 (2008).
23. Scheffer, M. *et al.* Early-warning signals for critical transitions. *Nature* **461,** 53–59 (2009).
24. Otto, A. *et al.* Energy budget constraints on climate response. *Nat. Geosci.* **6,** 415–416 (2013).
25. Lewis, N. & Curry, J. A. The implications for climate sensitivity of AR5 forcing and heat uptake estimates. *Clim. Dyn.* **45,** 1009–1023 (2015).
26. Marvel, K. *et al.* Implications for climate sensitivity from the response to individual forcings. *Nat. Clim. Chang.* **6,** 386–389 (2015).
27. Sherwood, S. C., Bony, S. & Dufresne, J.-L. Spread in model climate sensitivity traced to atmospheric convective mixing. *Nature* **505,** 37–42 (2014).
28. Cowtan, K. & Way, R. G. Coverage bias in the HadCRUT4 temperature series and its impact on recent temperature trends. *Q. J. R. Meteorol. Soc.* **140,** 1935–1944 (2014).

Acknowledgements This work was supported by the European Research Council (ERC) ECCLES project, grant agreement number 742472 (P.M.C.); the EU Horizon 2020 Research Programme CRESCENDO project, grant agreement number 641816 (P.M.C. and M.S.W.); the EPSRC-funded ReCoVER project (M.S.W.); and the NERC CEH National Capability fund (C.H.). We also acknowledge the World Climate Research Programme's Working Group on Coupled Modelling, which is responsible for CMIP, and we thank the climate modelling groups (listed in Extended Data Table 1 of this paper) for producing and making available their model output.

Author Contributions All authors collaboratively designed the study and contributed to the manuscript. P.M.C. led the study and drafted the manuscript. C.H. was the lead on the time-series data for the CMIP5 models. M.S.W. led on the theoretical analysis.

Author Information Reprints and permissions information is available at www.nature.com/reprints. The authors declare no competing financial interests. Readers are welcome to comment on the online version of the paper. Publisher's note: Springer Nature remains neutral with regard to jurisdictional claims in published maps and institutional affiliations. Correspondence and requests for materials should be addressed to P.M.C. (p.m.cox@exeter.ac.uk).

Reviewer Information *Nature* thanks P. Forster and T. Mauritsen for their contribution to the peer review of this work.

METHODS

Theoretical basis for the emergent relationship. We hypothesize that equation (1) (the 'Hasselmann model') is a reasonable approximation to the short-term variability of the global mean temperature anomaly ΔT:

$$C\frac{\mathrm{d}\Delta T}{\mathrm{d}t}+\lambda\Delta T=Q \tag{3}$$

If trends arising from net radiative forcing and ocean heat uptake can be successfully removed, the net radiative forcing term Q can be approximated by white noise. Under these circumstances, equation (1) is essentially the Ornstein–Uhlenbeck equation, which describes Brownian motion, and has standard solutions (for example, see https://en.wikipedia.org/wiki/Ornstein–Uhlenbeck_process) for the lag-one-year autocorrelation of the temperature:

$$\alpha_{1T}=\exp\left\{-\frac{\lambda}{C}\right\} \tag{4}$$

and the ratio of the variances of T and Q:

$$\frac{\sigma_T^2}{\sigma_Q^2}=\frac{1}{2\lambda C} \tag{5}$$

These two equations can be combined to eliminate the unknown heat capacity C and therefore to provide an expression for the climate feedback factor λ:

$$\lambda=\left\{\frac{\sigma_Q}{\sigma_T}\right\}\sqrt{-\frac{1}{2}\log_e\alpha_{1T}} \tag{6}$$

The ECS and λ are inversely related by a constant of proportionality, which is the radiative forcing due to doubling of atmospheric CO_2 ($Q_{2\times CO2}$), so that $\mathrm{ECS}=Q_{2\times CO2}/\lambda$. Thus, we can also derive an expression for ECS in terms of the variability of T and Q:

$$\mathrm{ECS}=Q_{2\times CO2}\left\{\frac{\sigma_T}{\sigma_Q}\right\}\sqrt{\frac{2}{-\log_e\alpha_{1T}}} \tag{7}$$

Least-squares linear regression. Least-squares linear regressions were calculated using well established formulae (see for example http://mathworld.wolfram.com/LeastSquaresFitting.html). The linear regression f_n between a time series given by y_n and a time series given by x_n is defined by a gradient b and intercept a:

$$f_n=a+bx_n \tag{8}$$

Minimizing the least-squares error for y_n involves minimizing:

$$s^2=\frac{1}{N-2}\sum_{n=1}^{N}\{y_n-f_n\}^2 \tag{9}$$

where N is the number of data points in each time series. In this case, the best-fit gradient is given by:

$$\bar{b}=\frac{\sigma_{xy}^2}{\sigma_x^2} \tag{10}$$

Here $\sigma_x^2=\sum_{n=1}^{N}\{x_n-\bar{x}\}^2/N$ is the variance of x_n and $\sigma_{xy}^2=\sum_{n=1}^{N}\{x_n-\bar{x}\}\times\{y_n-\bar{y}\}/N$ is the covariance of the x_n and y_n time series, with means of $\bar{x}$ and $\bar{y}$, respectively. The standard error of b is given by:

$$\sigma_b=\frac{s}{\sigma_x\sqrt{N}} \tag{11}$$

which defines a Gaussian probability density for b:

$$P(b)=\frac{1}{\sqrt{2\pi\sigma_b^2}}\exp\left\{-\frac{(b-\bar{b})^2}{2\sigma_b^2}\right\} \tag{12}$$

Finally, the 'prediction error' of the regression is the following function of x:

$$\sigma_f(x)=s\sqrt{1+\frac{1}{N}+\frac{\{x-\bar{x}\}^2}{N\sigma_x^2}} \tag{13}$$

This expression defines contours of equal probability density around the best-fit linear regression, which represent the probability density of y given x:

$$P\{y|x\}=\frac{1}{\sqrt{2\pi\sigma_f^2}}\exp\left\{-\frac{(y-f(x))^2}{2\sigma_f^2}\right\} \tag{14}$$

where $\sigma_f=\sigma_f(x)$, as described above.

Calculation of the PDF for ECS. The emergent constraint derived in this study is a linear regression across the CMIP5 models between ECS and the Ψ statistic of the de-trended global temperature. In the context of the least-squares linear regression presented above, ECS is equivalent to y, and Ψ is equivalent to x. The linear regression therefore provides an equation for the probability of ECS given Ψ (that is, the equation for $P\{y|x\}$ above). In addition, the Ψ statistic calculated from the de-trended observational dataset provides an observation-based PDF for Ψ. Given these two PDFs, $P\{\mathrm{ECS}|\Psi\}$ and $P(\Psi)$, the PDF for ECS is calculated by numerically integrating:

$$P(\mathrm{ECS})=\int_{-\infty}^{\infty}P\{\mathrm{ECS}|\Psi\}\,P(\Psi)\mathrm{d}\Psi \tag{15}$$

Data availability. The datasets generated during the current study are available from the corresponding author on reasonable request.

Code availability. The Python code used to produce the figures in this paper is available from the corresponding author on reasonable request.

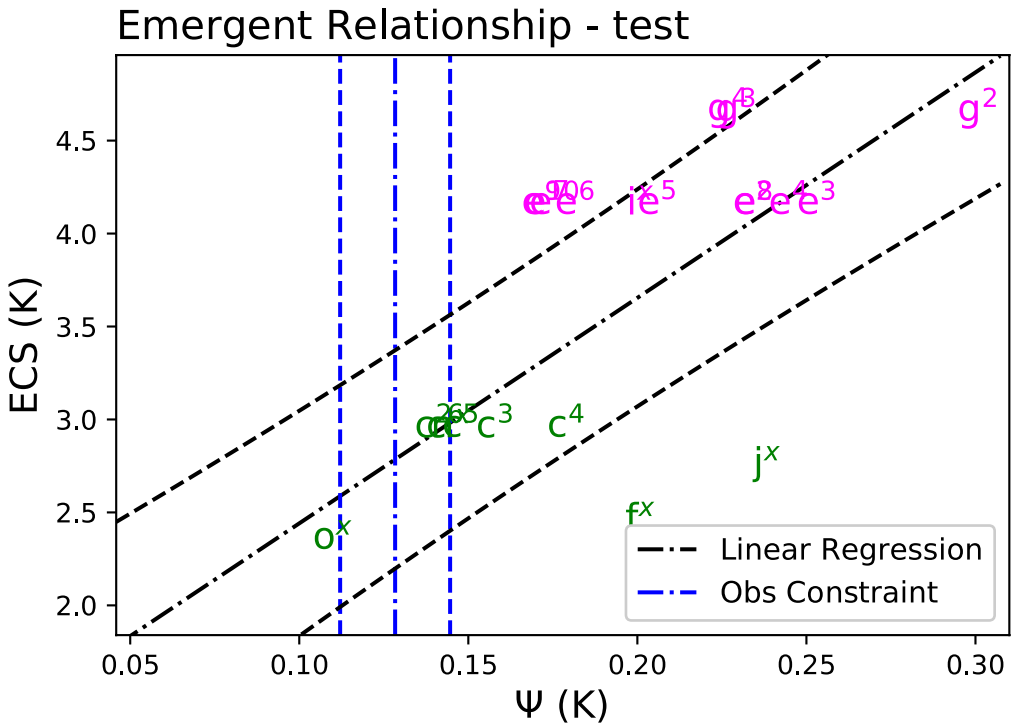

Extended Data Figure 1 | Test of emergent relationship against models not used in the calibration. The test set includes additional models from some climate centres (labelled 'f^x', 'f^y' and so on), and initial condition ensembles with particular models (labelled 'c^2', 'c^3' and so on). The black dot-dashed line shows the best-fit linear regression across the model ensemble, with the prediction error for the fit given by the black dashed lines (see Methods). The vertical blue lines show the observational constraint from the HadCRUT4 observations: the mean (dot-dashed line) and the mean plus and minus one standard deviation (dashed lines). Individual CMIP5 model runs are denoted by the letters listed in Extended Data Table 1.

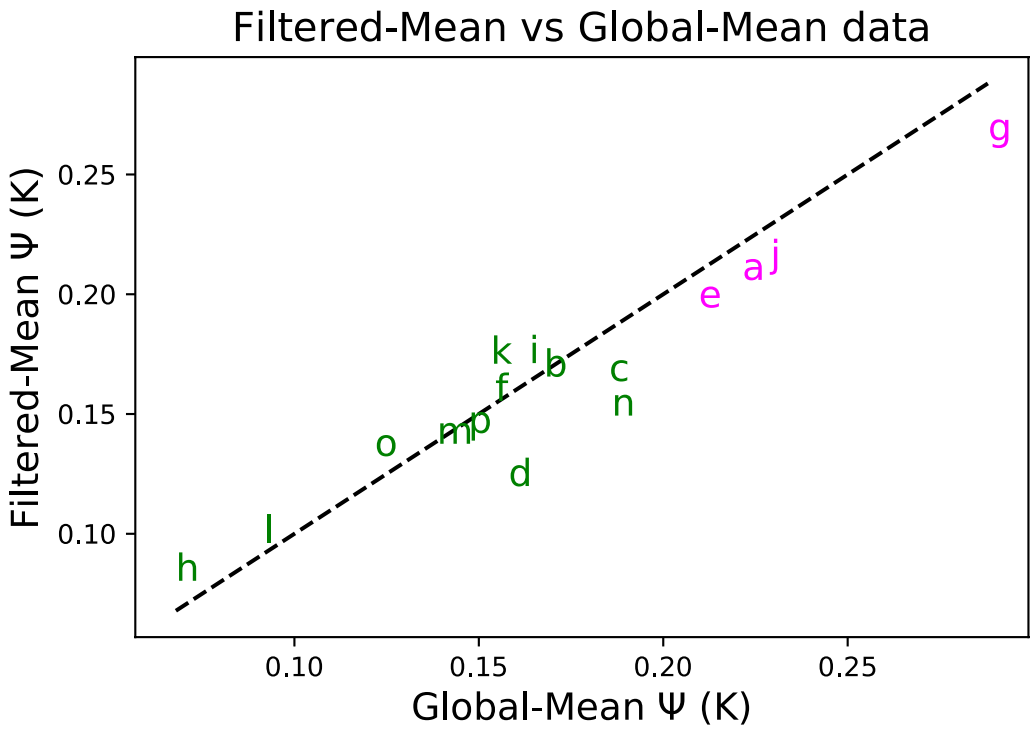

Extended Data Figure 2 | Comparison of Ψ statistics for the 16 CMIP5 models from 'filtered-mean' temperature and global-mean temperature. The filtered model output calculates area-mean values of temperature using only the points where there are observations in the HadCRUT4 dataset. All cases analyse 1880–2016 and use a 55-yr window width. The dotted line is the 1:1 line.

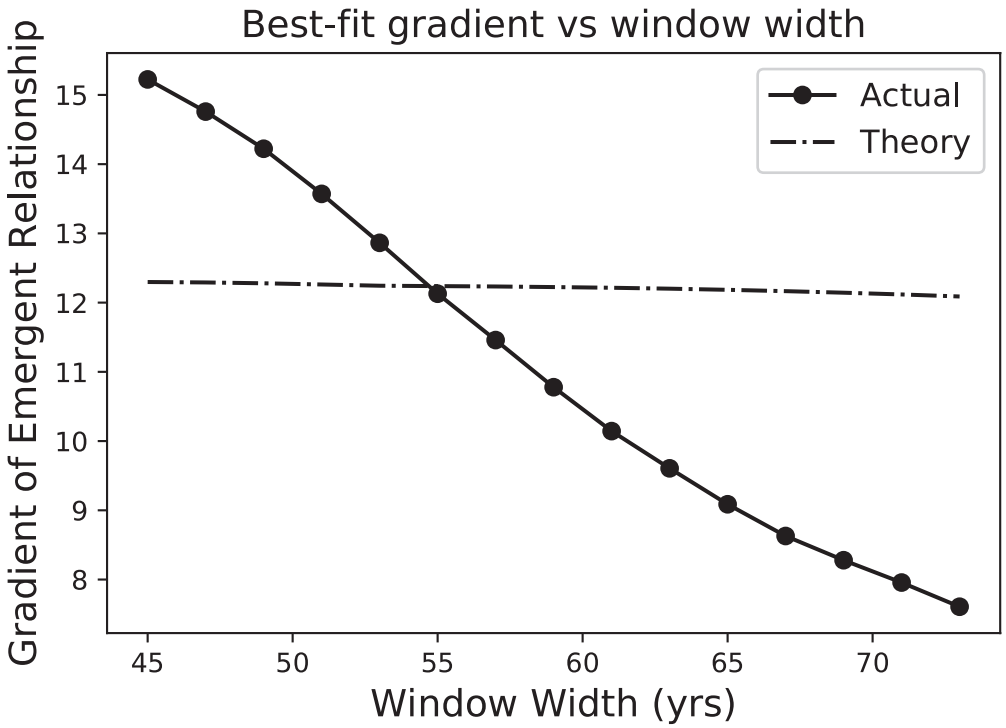

Extended Data Figure 3 | Gradient of emergent relationship between ECS and Ψ as a function of window width. The dotted line shows the gradient predicted with equation (2) using the ensemble-mean value of $Q_{2\times CO2}/\sigma_N$. Note that the theory (dot-dashed line) fits best at the optimal window width of 55 yr. All cases here analyse 1880–2016 and use the 16-model ensemble.

Extended Data Table 1 | Earth system models used in this study, as provided by the CMIP5 project[19]

	Model	λ (Wm^{-2} K^{-1})	*ECS* (K)	Q_{2xCO2}/σ_N	Ψ (K)
a	ACCESS1-0	0.8	3.8	8.5	0.22
b	CanESM2	1.0	3.7	8.3	0.17
c	CCSM4	1.2	2.9	7.3	0.19
d	CNRM-CM5	1.1	3.3	8.7	0.16
e	CSIRO-MK3-6-0	0.6	4.1	6.1	0.21
f	GFDL-ESM2M	1.4	2.4	5.9	0.15
g	HadGEM2-ES	0.6	4.6	7.8	0.29
h	inmcm4	1.4	2.1	11.9	0.07
i	IPSL-CM5B-LR	1.0	2.6	7.2	0.16
j	MIROC-ESM	0.9	4.7	11.7	0.23
k	MPI-ESM-LR	1.1	3.6	11.9	0.15
l	MRI-CGCM3	1.2	2.6	9.3	0.09
m	NorESM1-M	1.1	2.8	7.8	0.14
n	bcc-csm1-1	1.1	2.8	6.9	0.19
o	GISS-E2-R	1.8	2.1	11.1	0.12
p	BNU-ESM	1.0	4.1	8.0	0.15
f^{x}	GFDL-ESM2G	1.3	2.4	7.1	0.20
f^{y}	GFDL-CM3	0.8	4.0	6.7	0.36
i^{x}	IPSL-CM5A-LR	0.8	4.1	8.6	0.20
j^{x}	MIROC5	1.5	2.7	10.2	0.23
n^{x}	bcc-csm1-1-m	1.2	2.9	7.4	0.14
o^{x}	GISS-E2-H	1.7	2.3	11.8	0.10

The first column shows the symbol used for each model in Figs 1b and 2b. The third and fourth columns list λ and the ECS values as given in IPCC AR5 table 9.5 (ref. 17). The fifth and sixth columns show statistics calculated in this study for the period 1880–2016 and using a window width of 55 yr. The fifth column shows the ratio of the radiative forcing due to doubling CO_2 ($Q_{2\times CO2}$) to the standard deviation of the net top-of-atmosphere flux σ_N; and the sixth column shows the time-mean Ψ statistic for each model.

Extended Data Table 2 | Robustness of the emergent constraint to the choice of observational dataset and model ensemble

Observational Dataset	Obs. Constraint on Ψ (K)	Number of Models	Best estimate *ECS* (K)	'Likely' range *ECS* (K)
HadCRUT4	0.13 +/- 0.016	16	2.79	2.19 - 3.37
NOAA	0.16 +/- 0.034	16	3.13	2.45 - 3.81
Berkeley Earth	0.13 +/- 0.021	16	2.79	2.16 - 3.39
GISSTEMP	0.12 +/- 0.025	16	2.66	2.00 - 3.28
ALL	0.13 +/- 0.029	16	2.85	2.18 - 3.49
HadCRUT4	0.13 +/- 0.016	16; filtered	2.82	2.19 - 3.43
HadCRUT4	0.13 +/- 0.016	22	2.82	2.16 - 3.47
HadCRUT4	0.13 +/- 0.016	39	2.96	2.34 - 3.56

The 'ALL' dataset takes the mean and standard deviation of the Ψ values for all four global-mean temperature datasets (by concatenating the individual Ψ time series). The 'filtered' model output calculates area-mean values of temperature just using the points where there are observations in the HadCRUT4 dataset[27]. All cases analyse 1880–2016 and use a 55-yr window width.